THE JOURNAL OF PHYSICAL CHEMISTRY C

Article

pubs.acs.org/JPCC

Förster-Induced Energy Transfer in Functionalized Graphene

Ermin Malic,*[,†] Heiko Appel,[†] Oliver T. Hofmann,[†] and Angel Rubio*[,†,‡]

[†]Fritz-Haber-Institut der Max-Planck-Gesellschaft, Faradayweg 4-6, D-14195 Berlin, Germany

[‡]Nano-Bio Spectroscopy Group and ETSF Scientific Development Centre, Universidad del Pais Vasco, Avenida de Tolosa 72, E-20018 Donostia, Spain

ABSTRACT: Carbon nanostructures are ideal substrates for functionalization with molecules since they consist of a single atomic layer giving rise to an extraordinary sensitivity to changes in their surrounding. The functionalization opens a new research field of hybrid nanostructures with tailored properties. Here, we present a microscopic view on the substrate−molecule interaction in the exemplary hybrid material consisting of graphene functionalized with perylene molecules. First experiments on similar systems have been recently realized illustrating an extremely efficient transfer of excitation energy from adsorbed molecules to the carbon substrate, a process with a large application potential for high-efficiency photovoltaic devices and biomedical imaging and sensing. So far, there has been no microscopically founded explanation for the observed energy transfer. Based on first-principle calculations, we have explicitly investigated the different transfer mechanisms revealing the crucial importance of Förster coupling. Due to the efficient Coulomb interaction in graphene, we obtain strong Förster rates in the range of 1/fs. We investigate its dependence on the substrate−molecule distance R and describe the impact of the momentum transfer q for an efficient energy transfer. Furthermore, we find that the Dexter transfer mechanism is negligibly small due to the vanishing overlap between the involved strongly localized orbital functions. The gained insights are applicable to a variety of carbon-based hybrid nanostructures.

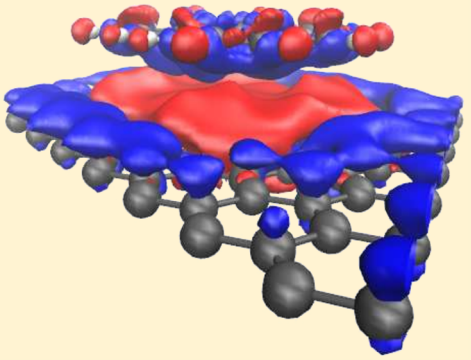

The continuing trend to miniaturization of devices in modern technology leads to fundamental physical limits of applied materials.[1,2] The search for new materials and new functionalities brings hybrid systems into the focus of current research.[3,4] They consist of low-dimensional nanostructures functionalized with single molecules combining the remarkable properties of both subsystems. In particular, carbon nanostructures are excellent substrates, since they offer a variety of metallic and semiconducting systems showing a large sensitivity to changes in their surrounding.[5−9] Noncovalent functionalization based on $\pi-\pi$ stacking preserves the intrinsic properties of the substrate to a large extent.[10] At the same time, the interaction with the attached molecules induces additional properties desired for specific technological applications.[11−19]

First experiments have been realized illustrating the successful functionalization of carbon nanotubes with photoactive molecules suggesting the design of efficient carbon-based molecular switching.[11,13,20−22] Recently, a strong excitation energy transfer has been observed in perylene- and porphyrin-functionalized carbon nanotubes suggesting efficient photodetection and light harvesting.[23−25] First studies on functionalized graphene also reveal high energy transfer rates between the attached molecules and the graphene layer.[26] The combination of unique transport properties of graphene, including ballistic transport and strong light absorption of organic molecules, results in new hybrid nanostructures with large application potential for high-efficiency photodetectors, biomedical sensors, and photovoltaic devices.[26]

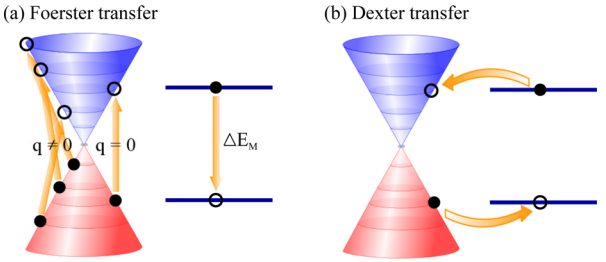

Figure 1. Schematic illustration of the nonradiative (a) Förster[27] and (b) Dexter[28] energy transfer in perylene-functionalized graphene. The Dirac cone represents the electronic band structure of graphene, while the electronic states of the perylene molecules are described by a two-level (HOMO−LUMO) momentum independent system. The arrows in (a) show different energy-conserving processes involving varying momentum transfer q.

The observed energy transfer could be explained by two major nonradiative energy transfer mechanisms (as depicted in Figure 1):[29] (i) Förster coupling[27] describes a direct transfer of energy from the optically excited molecule to graphene. This leads to a quenching of the molecular emission, since the energy is nonradiatively transferred to the electrons in graphene, see Figure 1a. The Förster transfer rate strongly

Received: February 25, 2014
Revised: April 6, 2014
Published: April 7, 2014

   dx.doi.org/10.1021/jp5019636 | J. Phys. Chem. C 2014, 118, 9283−9289

depends on the molecular transition dipole moment **d** and it exhibits a R^{-4} dependence for hybrid nanostructures on top of a spatially extended two-dimensional substrate[26,30] (in contrast to the well-known R^{-6} scaling for dipolar Förster coupling in molecule−molecule complexes). (ii) Dexter coupling[28] is based on a charge transfer between the molecule and graphene states, see Figure 1b. After the process, the molecule is brought into its ground state, and graphene becomes excited and can emit light through carrier recombination. It is a short-range transfer mechanism that directly depends on the spatial overlap of involved molecule and graphene orbital functions resulting in an exponential decay with the substrate−molecule distance *R*.

Recent studies indicate that the observed energy transfer in carbon-based hybrid nanostructures can probably be traced back to a Förster-like transfer process.[26,31] In these studies, the molecule−substrate distance is clearly larger than 10 Å due to the presence of long nonconducting linker molecules. However, for functionalization procedures without such additional molecules, the distance is in the range of just a few Å corresponding to the van der Waals radius of the involved atoms.[23] Here, the Dexter transfer mechanism is expected to be a competing energy transfer mechanism. In this Article, we present a systematic first-principle study on the substrate−molecule interaction in the exemplary hybrid system consisting of graphene functionalized with perylene molecules. The obtained insights should be applicable to other carbon-based hybrid nanostructures. We study the molecule-induced changes in the electronic band structure and the optical properties of graphene as well as the charge rearrangements within the two subsystems. Combining first-principle calculations characterizing the hybrid material with tight-binding-based calculations of the Förster transfer rate, we obtain an analytic expression allowing us to explicitly determine the strenght of the Förster coupling. To address the question which transfer mechanism is likely to be responsible for the efficient energy transfer observed in experiments on carbon-based hybrid materials,[23,26,31] we discuss the competing Dexter transfer mechanism by estimating the spatial overlap of the involved substrate and molecule orbitals within first-principle calculations.

The investigations are based on density functional theory (DFT) calculations performed within the FHI-aims code package.[32] It is an all-electron, full-potential electronic structure code, including numerical atom-centered orbitals, which are very efficient allowing the investigation of structures containing hundreds of atoms. All calculations are done within the tight settings including a tier 2 basis set for the carbon and hydrogen atoms.[32] Calculations with increased accuracy in the basis functions revealed that the chosen settings already lead to converged results with respect to the total energy. We focus on graphene functionalized with perylene molecules ($C_{20}H_{12}$), see Figure 2a,b, illustrating the top and side view of the studied structure. For graphene, we choose a supercell covering 7 × 7 unit cells corresponding to 98 carbon atoms, with a lattice constant of 1.42 Å. The investigated situation corresponds to a moderate functionalization degree with a molecule−molecule distance of approximately 7 Å. The electron interactions are described within the PBE exchange-correlation functional,[33] including the recently implemented van der Waals correction[34] to account for the long-range van der Waals interaction. The latter plays a fundamental role in describing the weak molecule−nanostructure coupling that is of paramount importance to quantitative estimate the relative contribution of the Dexter transfer mechanism. We also performed

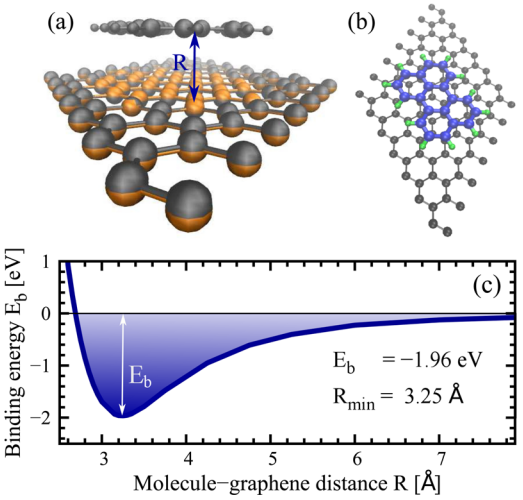

Figure 2. (a) Perylene-functionalized graphene after full geometric relaxation within the FHI-aims code including the van der Waals interaction. For comparison, the initial position of carbon atoms within a perfectly flat graphene layer is shown in orange illustrating a slight dent of the graphene layer in the vicinity of the molecule after the geometric relaxation. (b) Top view on the relaxed hybrid nanostructure emphasizing the structure of the perylene molecule. (c) The binding energy E_b as a function of the substrate−molecule distance *R*.

additional calculations with the hybrid functional PBE0[35] and HSE06[36,37] to investigate the alignment of molecular levels. We found that the molecular HOMO (LUMO) level is located below (above) the Fermi energy in graphene and, thus, initial spurious charge transfer does not occur.

The initial perylene-functionalized graphene structure is fully relaxed using the Broyden−Fletcher−Goldfarb−Shanno method minimizing all force components to values smaller than 10^{-3} eV/Å. Figure 2a illustrates the hybrid nanostructure after geometric relaxation. The comparison with the perfectly flat graphene layer (orange color) reveals a slight dent of carbon atoms of less than 0.1 Å close to the molecule. This geometric pillow effect is a direct consequence of the presence of the perylene molecule and can be traced back to the Pauli pushback.[38,39] It also gives rise to a charge rearrangement, which will be discussed below.

We find an optimal substrate−molecule distance of R_{min} = 3.25 Å, which is slightly smaller than the initial value of the van der Waals diameter of the carbon atom, see Figure 2c. The optimal binding energy at R_{min} is E_b = −1.96 eV corresponding to a binding energy of E_b = −61 meV per atom in the perylene molecule. This is in the expected range for a van der Waals-induced noncovalent adsorption of the molecule to the graphene surface. The π-electronic system of the perylene molecule is linked to the graphene surface via $\pi-\pi$ stacking, which is much less invasive compared to the covalent adsorption.[3] This can be well observed on the only minor changes in the electronic structure of the substrate, see Figure 3. Our calculations clearly illustrate that the unique band structure of graphene, including the Dirac point and the linear bands, is entirely preserved after the noncovalent functionalization with perylene molecules. The observable changes appear at the points where the molecular HOMO and LUMO levels cross the graphene electronic states, as illustrated in the inset of Figure 3. Here, the resulting states of the hybrid nanostructure exhibit avoided crossings. This well-known behavior in

dx.doi.org/10.1021/jp5019636 | J. Phys. Chem. C 2014, 118, 9283−9289

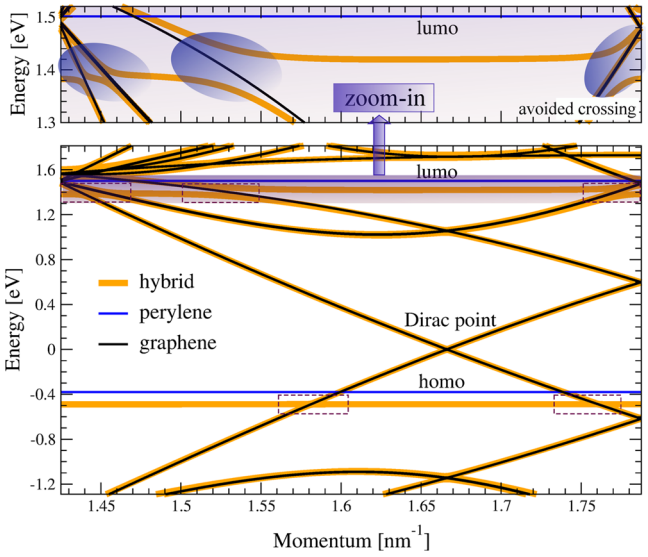

Figure 3. Bottom panel: Electronic band structure of the hybrid nanostructure (orange lines) in direct comparison to the band structure of unfunctionalized graphene (black lines) and isolated perylene molecules (blue lines). The electronic states remain largely unchanged except for the appearance of avoided crossings (dashed areas). Top panel: The region around the molecular LUMO level is zoomed-in to further illustrate this behavior.

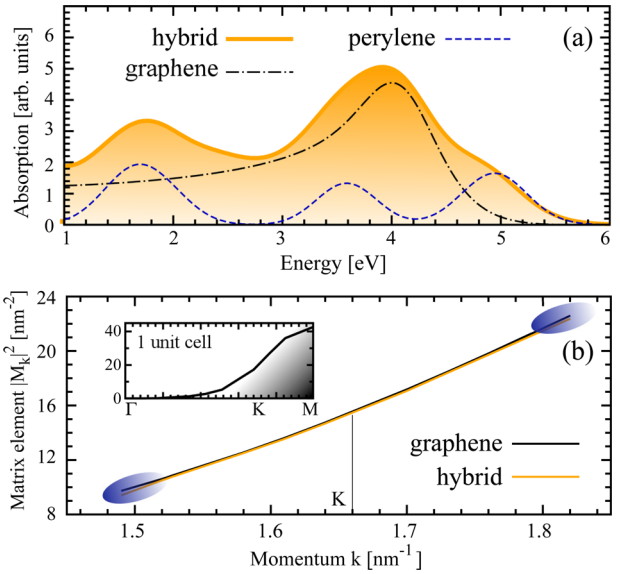

Figure 4. (a) Optical absorption of the perylene-functionalized graphene in comparison to the absorption of the pristine graphene and the isolated perylene molecule. (b) Optical matrix element describing the strength of matter−light coupling for the hybrid nanostructure and pristine graphene, respectively. The inset shows the matrix element along the high-symmetry line ΓKM within the Brillouin zone of one-unit-cell graphene.

quantum chemistry is further illustrated within the zoomed-in region around the molecular LUMO level, which anticrosses the graphene electronic states several times.

As a direct consequence of the almost completely preserved electronic band structure, the optical properties of graphene remain unchanged to a large extent, see Figure 4. The optical absorption of the hybrid nanostructure corresponds to an overlap of the absorption peaks of the pristine graphene and isolated perylene molecule, as shown in Figure 4a. The optical matrix element corresponding to the expectation value of the momentum operator[7] $\mathbf{M}_{\mathbf{k}}^{vc} = \langle \Phi_{\mathbf{k}}^{v} | \mathbf{p} | \Phi_{\mathbf{k}}^{c} \rangle$ exhibits only slight changes in the region, where avoided crossing takes place, see the blue-shaded circles in Figure 4b. Note, however, that the energy transfer within the hybrid nanostructure is not directly included within the DFT treatment and will be further discussed below.

The absorption spectrum of graphene is characterized by the well pronounced peak at approximately 4 eV corresponding to the transition at the saddle point (M point) in the Brillouin zone.[10,40,41] The widely delocalized π electronic system in the perylene molecule gives rise to strong absorption peaks at 1.7, 3.6, and 4.9 eV. The obtained transition energies are lower than in experiment due to the shortcoming of the applied exchange-correlation functional. Calculations based on hybrid functionals give a much better agreement with the experiment. Since in this work we focus on the Förster and Dexter energy transfer mechanisms between the perylene molecule and graphene, the energetic deviations within PBE exchange-correlation function do not play a qualitative role. Due to the linear gapless band structure of graphene in the relevant energy region, there are always electronic states that are in resonance with the energetically lowest HOMO−LUMO transition of the perylene molecule.

Furthermore, we have investigated the charge rearrangement within the hybrid nanostructure. As already seen in Figure 2, the adsorbed molecule leads to a spatial pillow-like effect[42] pushing the graphene's carbon atoms further away and giving rise to a small dent of <0.1 Å. This also affects the mobility of charge carriers within the graphene layer resulting in charge rearrangements. Figure 5a shows a surface plot illustrating the molecule-induced charge density difference $\Delta\rho(x,y,z) = \rho_{\text{hybrid}} - \rho_{\text{graphene}} - \rho_{\text{perylene}}$ for the exemplary iso-value of $5 \times 10^{-4}\ e_0/\text{Å}^3$. One can clearly see the accumulation of negative (blue) and positive (red) charges. According to the pillow effect, the electrons are pushed away from the region directly below the molecule. As a result, this region is characterized by a positive charge, that is, the lack of electrons (red areas). At the same time, electrons accumulate further away at the graphene surface at the graphene-facing side of the molecule (blue areas). To further illustrate the charge distribution along the z-direction (perpendicular to the graphene surface), we show the plane-averaged charge density difference $\Delta\rho(z) = \int dx \int dy \Delta\rho(z)$ and the charge difference $\Delta q(z) = \int_{-\infty}^{z} dz' \Delta\rho(z')$, see Figure 5b and c, respectively. The charge distribution around the graphene layer qualitatively reflects the spatial shape of the most relevant $2p_z$ carbon orbitals reaching above and below the graphene sheet. A similar charge distribution can also be observed around the position of the perylene molecule, illustrating a positive (negative) charge accumulation slightly below (above) the molecule. Note, however, that the quantitative effect of charge rearrangements is relatively small. The predicted small charge difference of up to 0.02 e_0 is in agreement with what one would expect for a noncovalent functionalization.

The dashed lines in Figure 5 reflect the charge distribution obtained within constrained DFT calculations,[43] that is, we imposed particular initial occupations of molecular HOMO and LUMO levels while solving the Kohn−Sham equations. The aim was to investigate the change of the substrate−molecule interaction once the molecule is optically excited. Therefore, we promoted one electron from the HOMO to the LUMO level.

dx.doi.org/10.1021/jp5019636 | J. Phys. Chem. C 2014, 118, 9283−9289

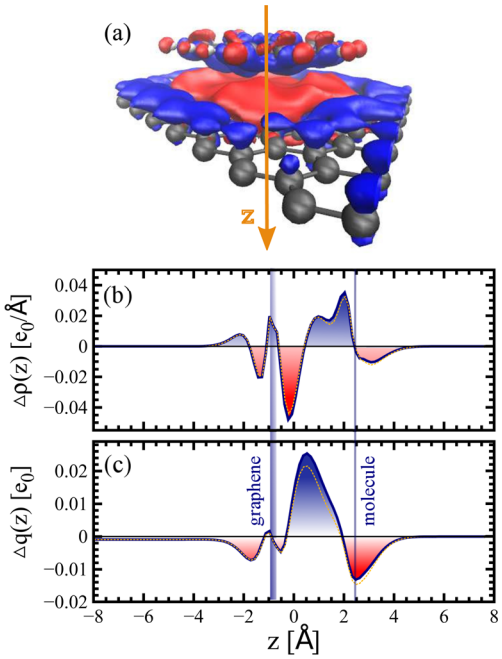

Figure 5. Charge density difference $\Delta\rho(x,y,z)$ is illustrated within a surface plot for the exemplary iso-value of $\pm 5 \times 10^{-4}$ $e_0/\text{Å}^3$. The red color corresponds to the negative value describing the lack of electrons, while the blue color reflects electron accumulations. (b) Charge density difference $\Delta\rho(z)$ integrated over the xy-plane illustrating the change of $\Delta\rho$ along the z-axis perpendicular to the graphene layer. (c) Charge difference $\Delta q(z) = \int_{-\infty}^{z} dz' \Delta\rho(z')$ accumulated along the z-axis as a function of z. The dashed lines correspond to the result obtained within constrained DFT calculations.

The calculations show only marginal changes in the charge distribution (cf., Figure 5) or in the electronic band structure (not shown). This insight is important for the discussion of the excitation energy transfer in the investigated hybrid structure. Time-dependent DFT calculations[44] are beyond the scope of this study and will be performed in future work.

After having characterized the perylene-functionalized graphene including its electronic and optical properties, we now focus on the investigation of the possible energy transfer mechanisms in such a hybrid structure, cf. Figure 1. To achieve this goal, we will combine the DFT-based knowledge of the hybrid material with the tight-binding-based analytic expression for the Förster transfer rate. Furthermore, we will discuss the Dexter transfer by exploiting our DFT study allowing us to estimate the overlap of the involved molecular and graphene orbitals.

The Förster and Dexter energy transfer rates can be analytically expressed via the Fermi golden rule

$$\gamma = \frac{2\pi}{\hbar} \sum_{\mathbf{k}_i} \sum_{\mathbf{k}_f} |V(v\mathbf{k}_i, c\mathbf{k}_f, l, h)|^2 \delta(\varepsilon^c_{\mathbf{k}_f} - \varepsilon^v_{\mathbf{k}_i} - \Delta E_M) \tag{1}$$

with the momentum-dependent initial and final states of the graphene substrate $\Phi^{\lambda}_{\mathbf{k}_i/\mathbf{k}_f}(\mathbf{r})$ and the HOMO and LUMO states of the molecule $\Phi^{l/h}_M(\mathbf{r})$. The delta function makes sure that only energy-conserving processes contribute. The Förster rate γ_F is determined by the direct contribution of the Coulomb interaction[27]

$$V_F(v\mathbf{k}_i, c\mathbf{k}_f, l, h) = \frac{e_0^2}{4\pi\varepsilon_0} \int d\mathbf{r} \int d\mathbf{r}' \Phi^{v*}_{\mathbf{k}_i}(\mathbf{r}) \Phi^{c}_{\mathbf{k}_f}(\mathbf{r}) \times \frac{1}{|\mathbf{r} - \mathbf{r}'|} \Phi^{l*}_M(\mathbf{r}') \Phi^{h}_M(\mathbf{r}') \tag{2}$$

where e_0 denotes the elementary charge and ε_0 the vacuum permittivity. The exchange Coulomb contribution gives the Dexter rate γ_D with[28]

$$V_D(v\mathbf{k}_i, c\mathbf{k}_f, l, h) = \frac{e_0^2}{4\pi\varepsilon_0} \int d\mathbf{r} \int d\mathbf{r}' \Phi^{v*}_{\mathbf{k}_i}(\mathbf{r}) \Phi^{h}_{M}(\mathbf{r}) \times \frac{1}{|\mathbf{r} - \mathbf{r}'|} \Phi^{l*}_M(\mathbf{r}') \Phi^{c}_{\mathbf{k}_f}(\mathbf{r}') \tag{3}$$

For Dexter coupling, a large spatial overlap between graphene and molecular orbitals ($\Phi^{v}_{\mathbf{k}_i}{}^*(\mathbf{r})\Phi^{h}_M(\mathbf{r})$ and $\Phi^{l}_M{}^*(\mathbf{r}')\Phi^{c}_{\mathbf{k}_f}(\mathbf{r}')$) is of key importance.[28,29] As a result, γ_D shows an exponential dependence on the substrate-molecule distance R and occurs only for small distances (typically, smaller than 10 Å).[29] In contrast, the Förster coupling is dominated by the factor $(1/(|\mathbf{r} - \mathbf{r}'|)$ in eq 2.

Considering the conventional energy transfer between donor and acceptor molecules, the Förster coupling is based on the dipole−dipole interaction and is characterized by a R^{-6} dependence.[27,29,45] In the case of functionalized graphene, the substrate is not a spatially localized molecule, but a periodically extended two-dimensional nanostructure. Following the approach of Swathi et al.,[30] the Förster coupling can be considered as an interaction of the molecular transition dipole $\mathbf{d}_M = -e_0 \int d\mathbf{r}' \Phi^{l}_M{}^*(\mathbf{r}') \mathbf{r}' \Phi^{h}_M(\mathbf{r}')$ located in the electrostatic potential $\varphi^{vc}_{\mathbf{k}_i,\mathbf{k}_f}(\mathbf{r}') = (1/(4\pi\varepsilon_0)) \int d\mathbf{r} (\rho^{vc}_{\mathbf{k}_i,\mathbf{k}_f}(\mathbf{r}))/(|\mathbf{r} - \mathbf{r}'|)$ arising from the transition charge density of graphene $\rho^{vc}_{\mathbf{k}_i,\mathbf{k}_f}(\mathbf{r}) = -e_0 \Phi^{v}_{\mathbf{k}_i}{}^*(\mathbf{r}) \Phi^{c}_{\mathbf{k}_f}(\mathbf{r})$. Then, the Förster energy transfer rate can be written as

$$\gamma_F = \frac{2\pi}{\hbar} \sum_{\mathbf{k}_i} \sum_{\mathbf{k}_f} |\mathbf{d}_M \cdot \nabla \varphi^{vc}_{\mathbf{k}_i,\mathbf{k}_f}|^2 \delta(\varepsilon^c_{\mathbf{k}_f} - \varepsilon^v_{\mathbf{k}_i} - \Delta E_M) \tag{4}$$

where the electrostatic potential $\varphi^{vc}_{\mathbf{k}_i,\mathbf{k}_f}$ is evaluated at the fixed position of the molecule.

Combining DFT calculations on the molecular transition dipole moment with the tight-binding approximation of the graphene wave functions allows us to obtain an analytic expression for γ_F. For the molecular transition dipole moment, we obtain $\mathbf{d}_M = (d_x, d_y, d_z) = (-0.80, 1.39, 4.92 \times 10^{-5})$ e_0 Å, with $d_M = 1.60$ e_0 Å. As expected for the flat perylene molecule lying in the x−y plane, d_z is nearly zero. The dipole moment is obtained for the perylene molecule that has been fully geometrically relaxed in the presence of the graphene substrate. Furthermore, we have also performed constrained DFT calculations[43] modeling an initially excited molecule (one electron promoted from the HOMO into the LUMO level) to account for the changes of the molecular states due to the optical excitation taking place before the actual energy transfer process, as illustrated in Figure 1. Our calculations reveal only negligibly small changes of the dipole components in agreement with the marginal changes observed for the charge distribution in Figure 5.

Within the tight-binding approximation, the transition charge density of graphene $\rho^{vc}_{\mathbf{k}_i,\mathbf{k}_f}(\mathbf{r})$ can be obtained analytically. Taking

dx.doi.org/10.1021/jp5019636 | J. Phys. Chem. C 2014, 118, 9283−9289

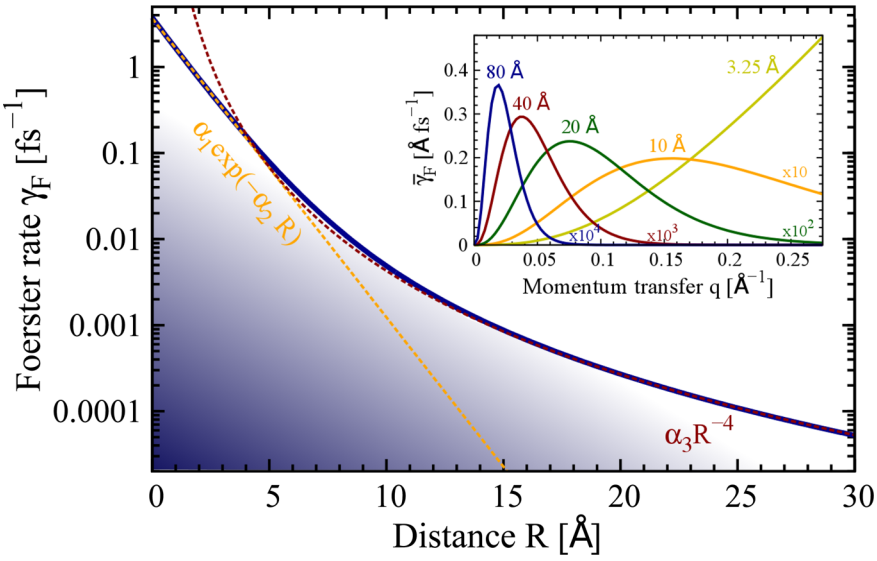

Figure 6. Förster energy transfer rate γ_F as a function of the substrate-molecule distance R. For short distances, the transfer rate is characterized by an exponential decay (orange line), while for large distances a R^{-4} behavior (red line) is found. The inset shows the momentum dependence of the processes contributing to the Förster transfer rate at different constant substrate−molecule distances R. Here, $\bar{\gamma}_F$ corresponds to the integrand of eq 5.

into account only the strongest overlaps one obtains for the Förster transfer rate[30]

$$\gamma_F(R) = \int_0^{\Delta E_M/\nu_F} \frac{e_0^2}{128\pi\hbar\varepsilon_0^2}(d_\parallel^2 + 2d_\perp^2)\frac{e^{-2qR}q^3}{\sqrt{\Delta E_M^2 - \nu_F^2 q^2}}\mathrm{d}q$$
$$\approx \begin{cases} \alpha_1 e^{-\alpha_2 R} & \text{for } R < 10 \text{ Å} \\ \alpha_3 R^{-4} & \text{for } R \gg 10 \text{ Å} \end{cases} \quad (5)$$

with the HOMO−LUMO gap ΔE_M and the slope in the electronic band structure of graphene ν_F. More details on the derivation of the Förster transfer rate can be found in the work of Swathi et al.[30] Here, we focus on the evaluation of this expression for the investigated perylene-functionalized graphene. The Förster coupling explicitly depends on the square of the parallel $d_\parallel$ (in the x−y plane) and the perpendicular component $d_\perp$ (z-axis) of the molecular transition dipole moment $\mathbf{d}_M$. Since we have already determined these characteristics for the perylene molecule within the graphene-based hybrid material, we can now explicitly evaluate the Förster energy transfer rate.

Figure 6 illustrates the Förster rate as a function of the substrate−molecule distance R. Generally, the integral over all processes involving the momentum transfer q cannot be analytically solved. We find that, within the simplest tight-binding approximation taking into account only the strongest overlaps, the direct transitions with $q = 0$ do not contribute to the energy transfer. The inset of Figure 6 shows the integrand of eq 5 (denoted as $\bar{\gamma}_F$) as a function of q for different fixed distances R. For $R < 10$ Å, $\bar{\gamma}_F(q)$ quickly increases with q and the Förster rate γ_F shows an exponential decay with R, that is, $\gamma_F \approx \alpha_1 e^{-\alpha_2 R}$ with $\alpha_1 \approx 3.66$ fs^{-1} and $\alpha_2 \approx 0.80$ Å^{-1}, see Figure 6. For large distances, the behavior drastically changes: $\bar{\gamma}_F(q)$ is characterized by a maximum centered at $q \approx 3/(2R)$, that is, only processes involving a certain momentum transfer q significantly contribute to the energy transfer rate. In the limit of large substrate−molecule distances ($R \gg 10$ Å), the Förster coupling exhibits a clear R^{-4} dependence, that is, $\gamma_F \approx \alpha_3 R^{-4}$, with $\alpha_3 \approx 42.85$ fs^{-1}, see Figure 6. This is in excellent agreement with the observations in a recent experiment varying the distance between graphene and attached molecular emitters by depositing additional layers.[26]

Inserting the molecular transition dipole moment $\mathbf{d}_M = (d_\perp, d_\parallel)$ for the investigated exemplary perylene-functionalized graphene, we obtain a very efficient Förster energy transfer rate of $\gamma_F(R_0) = 0.277$ fs^{-1}. This can be traced back to the strong Coulomb interaction in the graphene substrate and the short substrate−molecule distance of $R_0 = 3.25$ Å obtained within a full geometric relaxation of the entire hybrid nanostructure. At such a short distance, transitions involving different momentum transfers q crucially contribute to the Förster rate, see the inset of Figure 6. Our result is in line with experimental time-resolved investigations of the energy transfer in functionalized carbon nanotubes, suggesting that the transfer process occurs on an ultrafast femtosecond time scale.[46] Often, it is necessary to include additional linker molecules to experimentally achieve the functionalization[22] resulting in much larger substrate−molecule distances. For example, $R = 10$ and 50 Å result in a Förster rate of $\gamma_F = 4.88$ ps^{-1} and 6.88×10^{-3} ps^{-1}, respectively. The drastic decrease in efficiency is in agreement with the experimental findings of L. Gaudreau and co-workers.[26]

In spite of the short distance between the graphene layer and the perylene molecule, our calculations reveal that the Dexter energy transfer rate γ_D is negligibly small compared to the discussed Förster transfer mechanism. The Dexter rate is determined by the spatial overlap between the strongly localized graphene and perylene orbitals. To estimate γ_D, we calculate the ratio between the overlaps $\alpha_D = \langle \Phi_{\mathbf{k}_i}^{v*}(\mathbf{r}) | \Phi_M^h(\mathbf{r}) \rangle$ and $\alpha_F = \langle \Phi_{\mathbf{k}_i}^{v*}(\mathbf{r}) | \Phi_{\mathbf{k}_f}^{c}(\mathbf{r}) \rangle$ appearing in the Dexter and the Förster rate, respectively, see eqns 2 and 3. We obtain $\alpha_D/\alpha_F \approx 10^{-1}$. Since in the rates the square of the product of two such overlaps appears, the Dexter rate γ_D is expected to be approximately 4 orders of magnitude smaller than the Förster rate γ_F.

dx.doi.org/10.1021/jp5019636 | J. Phys. Chem. C 2014, 118, 9283−9289

In conclusion, we have investigated the energy transfer in perylene-functionalized graphene. Having characterized the hybrid material within DFT calculations including a fully geometric relaxation of the structure, its electronic band structure, optical properties, and charge rearrangements, we focus on the energy transfer that has been measured in recent experiments. Combining DFT-based calculation of the molecular transition dipole moment and tight-binding-based consideration of graphene wave functions allows us to obtain an analytic expression for the Förster energy transfer rate. Our calculations reveal strongly efficient Förster coupling with rates in the range of fs^{-1}. In contrast, the Dexter energy transfer mechanism is found to be negligibly small due to small overlap between the involved strongly localized substrate and molecule orbital functions. The obtained results can be applied to other carbon-based hybrid nanostructures and in general to the description of energy transfer processes in molecular functionalized nanostructures, once the molecular dipole moment and the substrate−molecule separation are known.

AUTHOR INFORMATION

Corresponding Authors

*E-mail: ermin.malic@tu-berlin.de.

*E-mail: angel.rubio@ehu.es.

Notes

The authors declare no competing financial interest.

ACKNOWLEDGMENTS

We thank the Einstein Foundation Berlin and the Deutsche Forschungsgemeinschaft (within the collaborative research center SFB 658) for financial support. O.T.H. acknowledges the support from FWF (Project: J 3285-N20). A.R. acknowledges financial support from the European Research Council (ERC-2010-AdG-267374), Spanish Grant (FIS2010-21282-C02-01), Grupos Consolidados UPV/EHU del Gobierno Vasco (IT578-13), and the EU Project (280879-2 CRONOS CP-FP7).

REFERENCES

(1) Avouris, P.; Chen, Z.; Perebeinos, V. Carbon-Based Electronics. *Nat. Nanotechnol.* **2007**, *2*, 605−615.

(2) Bonaccorso, F.; Sun, Z.; Hasan, T.; Ferrari, A. C. Graphene Photonics and Optoelectronics. *Nat. Photonics* **2010**, *4*, 611−622.

(3) Hirsch, A.; Vostrowsky, O. Functionalization of Carbon Nanotubes. *Top. Curr. Chem.* **2005**, *245*, 193−237.

(4) Burghard, M. Electronic and Vibrational Properties of Chemically Modified Single-Wall Carbon Nanotubes. *Surf. Sci. Rep.* **2005**, *58*, 1−109.

(5) Reich, S.; Thomsen, C.; Maultzsch, J. *Carbon Nanotubes: Basic Concepts and Physical Properties*; Wiley-VCH: Berlin, 2004.

(6) Jorio, A.; Dresselhaus, M.; Dresselhaus, G. *Carbon Nanotubes: Advanced Topics in the Synthesis, Structure, Properties, and Applications*; Springer: Berlin, 2008.

(7) Malić, E.; Knorr, A. *Graphene and Carbon Nanotubes: Ultrafast Optics and Relaxation Dynamics*; Wiley-VCH: Berlin, 2003.

(8) Avouris, P.; Freitag, M.; Perebeinos, V. Carbon-Nanotube Photonics and Optoelectronics. *Nat. Photonics* **2008**, *2*, 341−350.

(9) Malic, E.; Weber, C.; Richter, M.; Atalla, V.; Klamroth, T.; Saalfrank, P.; Reich, S.; Knorr, A. Microscopic Model of the Optical Absorption of Carbon Nanotubes Functionalized with Molecular Spiropyran Photoswitches. *Phys. Rev. Lett.* **2011**, *106*, 097401−097405.

(10) Malić, E.; Winzer, T.; Bobkin, E.; Knorr, A. Microscopic Theory of Absorption and Ultrafast Many-Particle Kinetics in Graphene. *Phys. Rev. B* **2011**, *84*, 205406−205420.

(11) Guo, X.; Huang, L.; O'Brien, S.; Kim, P.; Nuckolls, C. Directing and Sensing Changes in Molecular Conformation on Individual Carbon Nanotube Field Effect Transistors. *J. Am. Chem. Soc.* **2005**, *127*, 15045−15047.

(12) Sundaram, R. S.; Gomez-Navarro, C.; Balasubramanian, K.; Burghard, M.; Kern, K. Electrochemical Modification of Graphene. *Adv. Mater.* **2008**, *20*, 3050−3053.

(13) Zhou, X.; Zifer, T.; Wong, B. M.; Krafcik, K. L.; Leonard, F.; Vance, A. L. Color Detection Using Chromophore-Nanotube Hybrid Devices. *Nano Lett.* **2009**, *9*, 1028−1033.

(14) Ehli, C.; Oelsner, C.; Guldi, D. M.; Mateo-Alonso, A.; Prato, M.; Schmidt, C.; Backes, C.; Hauke, F.; Hirsch, A. Manipulating Single-Wall Carbon Nanotubes by Chemical Doping and Charge Transfer with Perylene Dyes. *Nat. Chem.* **2009**, *1*, 243−249.

(15) Charlier, J. M.; et al. Carbon Nanotubes Randomly Decorated with Gold Clusters: From Nano2hybrid Atomic Structures to Gas Sensing Prototypes. *Nanotechnology* **2009**, *20*, 375501−375511.

(16) Loi, M. A.; Gao, J.; Cordella, F.; Blondeau, P.; Menna, E.; Bartova, B.; Hebert, C.; Lazard, S.; Bottone, G. A.; Milko, M.; Ambrosch-Draxl, C. Encapsulation of Conjugated Oligomers in Single Wall Carbon Nanotubes: Towards Nano-Hybrids for Photonic Devices. *Adv. Mater.* **2010**, *22*, 1635−1639.

(17) Kolpak, A. M.; Grossman, J. C. Azobenzene-Functionalized Carbon Nanotubes As High-Energy Density Solar Thermal Fuels. *Nano Lett.* **2011**, *11*, 3156−3162.

(18) Berghäuser, G.; Malić, E. Molecule−Substrate Interaction in Functionalized Graphene. *Carbon* **2014**, *69*, 536−542.

(19) Berghäuser, G.; Malić, E. Optical Properties ofFunctionalized Graphene. *Phys. Status Solidi B* **2013**, *250*, 2678−2680.

(20) Simmons, J. M.; In, I.; Campbell, V. E.; Mark, T. J.; Léonard, F.; Gopalan, P.; Eriksson, M. A. Optically Modulated Conduction in Chromophore-Functionalized Single-Wall Carbon Nanotubes. *Phys. Rev. Lett.* **2007**, *98*, 086802−086806.

(21) Malić, E.; Setaro, A.; Bluemmel, P.; Sanz-Navarro, C. F.; Ordejon, P.; Reich, S.; Knorr, A. Carbon Nanotubes as Substrates for Molecular Spiropyran-Based Switches. *J. Phys.: Condens. Matter* **2012**, *24*, 394006−394012.

(22) Setaro, A.; Bluemmel, P.; Maity, C.; Hecht, S.; Reich, S. Non-Covalent Functionalization of Individual Nanotubes with Spiropyran-Based Molecular Switches. *Adv. Funct. Mater.* **2012**, *22*, 2425−2431.

(23) Magadur, G.; Lauret, J.-S.; Alain-Rizzo, V.; Voisin, C.; Roussignol, P.; Deleporte, E.; Delaire, J. A. Excitation Transfer in Functionalized Carbon Nanotubes. *ChemPhysChem* **2008**, *9*, 1250−1253.

(24) Roquelet, C.; Garrot, D.; Lauret, J. S.; Voisin, C.; Alain-Rizzo, V.; Roussignol, P.; Delaire, J. A.; Deleporte, E. Quantum Efficiency of Energy Transfer in Noncovalent Carbon Nanotube/Porphyrin Compounds. *Appl. Phys. Lett.* **2010**, *97*, 141918−141921.

(25) Ernst, F.; Heek, T.; Setaro, A.; Haag, R.; Reich, S. Energy Transfer in Nanotube-Perylene Complexes. *Adv. Funct. Mater.* **2012**, *22*, 3921−3926.

(26) Gaudreau, L.; Tielrooij, K. J.; Prawiroatmodjo, G. E.; Osmond, J.; de Abajo, F. J. G.; Koppens, F. H. Universal Distance-Scaling of Nonradiative Energy Transfer to Graphene. *Nano Lett.* **2013**, *13*, 2030−2035.

(27) Förster, T. Zwischenmolekulare Energiewanderung und Fluoreszenz. *Ann. Phys.* **1948**, *437*, 55−75.

(28) Dexter, D. L. A Theory of Sensitized Luminescence in Solids. *J. Chem. Phys.* **1953**, *21*, 836−850.

(29) Winkler, J. R. FRETting over theSpectroscopic Ruler. *Science* **2008**, *339*, 1530−1531.

(30) Swathi, R. S.; Sebastian, K. L. Distance Dependence of Fluorescence Resonance Energy Transfer. *J. Chem. Sci.* **2009**, *121*, 777−787.

(31) Ernst, F.; Heek, T.; Setaro, A.; Haag, R.; Reich, S. Excitation Characteristics of Different Energy Transfer in Nanotube-Perylene Complexes. *Appl. Phys. Lett.* **2013**, *102*, 233105−233110.

(32) Blum, V.; Gehrke, R.; Hanke, F.; Havu, P.; Havu, V.; Ren, X.; Reuter, K.; Scheffler, M. Ab Initio Molecular Simulations with

Numeric Atom-Centered Orbitals. *Comput. Phys. Commun.* **2009**, *180*, 2175−2196.
(33) Perdew, P.; Burke, K.; Ernzerhof, M. Generalized Gradient Approximation Made Simple. *Phys. Rev. Lett.* **1996**, *77*, 3865−3869.
(34) Tkatchenko, A.; Scheffler, M. Accurate Molecular van der Waals Interactions from Ground-State Electron Density and Free-Atom Reference Data. *Phys. Rev. Lett.* **2009**, *102*, 073005−073009.
(35) Adamo, C.; Barone, V. Toward Reliable Density Functional Methods without Adjustable Parameters: The PBE0 Model. *J. Chem. Phys.* **1999**, *110*, 6158−6170.
(36) Heyd, J.; Scuseria, G. E.; Ernzerhof, M. Hybrid Functionals Based on a Screened Coulomb Potential. *J. Chem. Phys.* **2003**, *118*, 8207−8215.
(37) Krukau, A. V.; Vydrov, O. A.; Izmaylov, A. F.; Scuseria, G. E. Influence of the Exchange Screening Parameter on the Performance of Screened Hybrid Functionals. *J. Chem. Phys.* **2006**, *125*, 224106−224111.
(38) Bagus, P. S.; Käfer, D.; Witte, G.; Wöll, C. Work Function Changes Induced by Charged Adsorbates: Origin of the Polarity Asymmetry. *Phys. Rev. Lett.* **2008**, *100*, 126101−126105.
(39) Hofmann, O. T.; Rangger, G. M.; Zojer, E. Reducing the Metal Work Function Beyond Pauli Pushback: A Computational Investigation of Tetrathiafulvalene and Viologen on Coinage Metal Surfaces. *J. Phys. Chem. C* **2008**, *112*, 20357−20365.
(40) Mak, K. F.; Shan, J.; Heinz, T. F. Seeing Many-Body Effects in Single- and Few-Layer Graphene: Observation of Two-Dimensional Saddle-Point Excitons. *Phys. Rev. Lett.* **2011**, *106*, 046401−046405.
(41) Chae, D.; Utikal, T.; Weisenburger, S.; Giessen, H.; Klitzing, K. v. Excitonic Fano Resonance in Free-Standing Graphene. *Nano Lett.* **2011**, *11*, 1379−1382.
(42) Hofmann, O. T.; Atalla, V.; Mollx, N.; Rinke, P.; Scheffler, M. Interface Dipoles of Organic Molecules on Ag(111) in Hybrid Density-Functional Theory. *New J. Phys.* **2013**, *15*, 123028−123053.
(43) Wu, Q.; Voorhis, T. V. Direct Optimization Method to Study Constrained Systems within Density-Functional Theory. *Phys. Rev. A* **2005**, *72*, 024502−024506.
(44) Hofmann-Mees, D.; Appel, H.; Ventra, M. D.; Kuemmel, S. Determining Excitation-Energy Transfer Times and Mechanisms from Stochastic Time-Dependent Density Functional Theory. *J. Phys. Chem. B* **2013**, *117*, 14408−14419.
(45) Baer, R.; Rabani, E. Theory of Resonance Energy Transfer Involving Nanocrystals: The Role of High Multipoles. *J. Chem. Phys.* **2008**, *128*, 184710−184722.
(46) Garrot, D.; Langlois, B.; Roquelet, C.; Michel, T.; Roussignol, P.; Delalande, C.; Deleporte, E.; Lauret, J.; Voisin, C. Time-Resolved Investigation of Excitation Energy Transfer in Carbon Nanotube-Porphyrin Compounds. *J. Phys. Chem. C* **2011**, *115*, 23283−23292.